Indian J Phys (November 2022) 96(13):3761–3773
https://doi.org/10.1007/s12648-022-02311-5

ORIGINAL PAPER

Structural stability, electronic, mechanical, and thermodynamic properties of the new MAX phases Mn_2SiC_1, Mn_3SiC_2 and Mn_4SiC_3: ab-initio calculations

F Keramsi[1], M Berber[2,3]*, M Mebrek[2] and A Mir[1,4]

[1]Département de Physique, Institut des Sciences de la Nature et de Vie & Sciences Exactes (SNV-SE), Université Ahmed ZABANA de Relizane, 48000 Relizane, Algeria

[2]Centre Universitaire Nour Bachir El Bayadh, 32000 El Bayadh, Algeria

[3]Laboratoire d'Instrumentation et Matériaux Avances, Centre Universitaire Nour Bachir El-Bayadh, BP 900 route, 32000 Aflou, Algérie

[4]Faculty of Sciences, Department of Physics, Dr. Tahar, Moulay University of Saida, 20000 Saida, Algeria

Received: 31 July 2021 / Accepted: 03 February 2022 / Published online: 10 March 2022

Abstract: In this work, we have studied the structural, electronic, elastic, and thermodynamic properties of the new Max phase's class Mn_2SiC_1, Mn_3SiC_2 and Mn_4SiC_3 ($Mn_{n+1}SiC_n$ with n = 1, 2 and 3), using the linearly augmented plane wave method (FP-LAPW) based on density functional theory. The exchange-correlation potential is treated with the local density approximation LSDA. The formation energies calculated for all compounds showed that these compounds are thermodynamically stable. We found that the ferromagnetic (FM) configuration is more stable than the non-magnetic (NM) one, at their lattice parameters for all three compounds. Cohesive energy confirms the structural stability of all structures. The total magnetic moment increases with an increasing value of n. The band structure indicates that the three materials are electrically conductive. For the density of state, we see that there is no gap for these three materials; they exhibit a metallic nature which results from the fact that the Mn-3d states are dominant at the Fermi level. The peak of hybridization of the Mn–3d, and C–2p states leads to a strong covalent bond than that between the Mn–3d and Si–3p states in the low energy domain. 3p electrons in silicon elements can effectively alter the covalence and iconicity of bonds that govern compressibility, ductility, and even superconducting properties. The chemical bond in three compounds is a combination of covalent, ionic, and metallic nature. The main factors governing the electronic properties are the hybrid states Mn–3d, Si–3p, and C–2p, and the bond (p–d) stabilizes the structure. The elastic constants are calculated and the conditions of the criterion of mechanical stability are checked. In addition, we have calculated the bulk, and shear modulus, Young's modulus, Poisson's ratio, and anisotropy index. The quasi-harmonic Debye model was used to study the temperature-dependent thermodynamic properties of the $Mn_{n+1}SiC_n$ (n = 1, 2, 3) compounds.

Keywords: DFT calculations; MAX phase materials; Ferromagnetic properties; Electronic structures; Elastic properties

1. Introduction

In the 1960s, Nowotny reported the discovery of more than 100 carbides and nitrides [1–3]. Among them, there are more than 30 so-called H- or Hagg phases [2, 3]. In the mid-1990s, a lot of researchers begin interest in this exploration again, most notably Barsoum and El-Raghy synthesized relatively phase-pure samples of Ti_3SiC_2 and revealed a material with a unique combination of metallic and ceramic properties [2, 4]. The known max phases, with the general formula $M_{n+1}AX_n$ where M is transition metal, A is a group IIIA or IVA element, and (X is C or N), and n = 1,2,3 [2, 3, 5]. For n = 1, this becomes the M_2AX phase and called the 211 Max phases characterized by the work of Jeitschko, Nowotny, Toth, and their collaborators in 1960 [6–8]. Likewise, the phases M_3AX_2 are the structure 312 [7] corresponding to the compounds of phase Max Hf_3AlC_2, and Ti_3AlC_2 [9, 10] for n = 2, and the structure M_4AX_3 or 413 exists for n = 3, [7] like M_4AlC_3 (M = V, Nb,

*Corresponding author, E-mail: berbermohamed@yahoo.fr

© 2022 IACS

and Ta), Ti_4AlN_3, Ti_4GaC_3 [11–13]. On the other hand, there are other Max phases with the stoichiometry of X_5AX_4, X_6AX_5, and X_7AX_6 have also been declared in the literature, importantly the number of max phases and their solid solutions are increasing rapidly [7]. Max Phases $M_{n+1}AX_n$ are crystallized in the hexagonal structure belonging to the space group of $D_{6h}^4 - P63/mmc$ with hexagonal unit cells [7], with nearly compact layers of M elements intertwined with flat square plates of pure A elements, where X atoms fill the octahedral sites between (M) atoms. The A elements are located at the center of trigonal prisms larger than the X octahedral sites. The structural difference between the three Max phases M_2AX, M_3AX_2, and M_4AX_3 can be observed in the number of monolayer's introduced for each M layer [14]. In addition, phases M_3AX_2 , and M_4AX_3 have two different M sites, denoting M_1 and M_2. Crystal structure M_4AX_3 also has two different X sites, named as X_1 and X_2, and has more carbide-like characteristics than crystal structures M_2AX , and M_3AX_2 [14]. Figure 1 shows the sketches of the 211, 312, 413 Max phases, according to the value of n. The Max phases are a class of solid with both ceramic and metallic properties, a rather unusual combination, this makes them attractive for many applications as structural materials at elevated temperatures [8]. In general, they are good thermal and electrical conductors, machinability, low hardness, thermal shock resistance, and damage tolerance, on the other hand, these materials have ceramic-like high elastic modulus, high melting temperature, and oxidation and corrosion resistance [8, 15–30]. These remarkable properties come from the layered structure of the Max phases and the mixed metallic covalent nature of the M-X bonds, which are exceptionally strong, combined with the relatively weak M-A bonds [31]. Max phases do not melt but decompose at high temperatures, decomposition produces the transition metal carbide or nitride and the group A element [3], max phases are used as a replacement for machinable ceramics, kiln furniture, wear, and corrosion protection, heat exchangers, applications where rotating parts are used, low friction, trainers for health products, hot pressing tools, and resistance heating elements [32, 33], and are appropriate for many technological applications as structural materials at elevated temperatures. Due to these important properties, max phases are studied experimentally and theoretically. Many researchers have been interested in recent years in studying these properties, and other properties of materials of the same family. According to the research, there is not a theoretical or experimental study on the max phases $Mn_{n+1}SiC_n$, $n = 1, 2, 3$. The objective of this new study is to predict the structural, electronic, elastic, and mechanical properties of Max phases $Mn_{n+1}SiC_n$, $n = 1, 2, 3$. Using the calculations of the first principle calculations of density functional theory [34, 35] within exchange and correlation potential of local spin density approximation LSDA [36]. These results could serve as support for future theoretical and experimental studies. This paper is organized as follows: the computational method and the details of calculations are described in Sect. 2, the results are discussed in Sect. 3, and we end this work with a conclusion

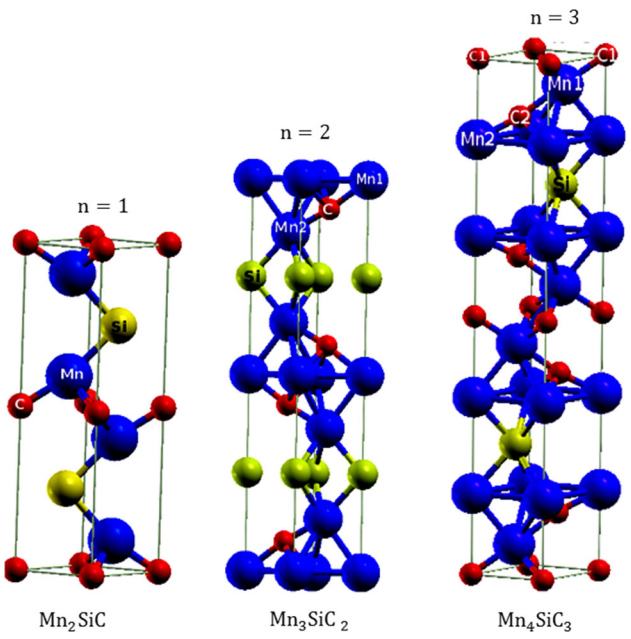

Fig. 1 Crystal structure of Mn_2SiC, Mn_3SiC_2, and Mn_4SiC_3

2. Calculation method

The structural, electronic, mechanical, and thermodynamic properties of these $M_{n+1}AX_n, (n = 1, 2, 3)$ compounds are calculated using the density functional theory (DFT) [34, 35] by employing the first-principles full-potential linearized augmented plane wave (FP-LAPW) method implemented in the Wien2k package [37]. LSDA was used for the exchange-correlation potential. The energy of separation between valence and core states was chosen – 7 Ry. We take $R_{MT} * K_{MAX}$ equal to 9 (where R_{MT} is the average radius of the muffin-tin sphere and K_{MAX} is the maximum value of the wave vector $(K = k + G)$. In these calculations, the radii R_{MT} of the muffin-tin spheres are set to 1.9, 1.86, and 1.53 a.u (atom unit) for Mn, Si, and C atoms, respectively. So that, the muffin-tin spheres do not overlap. Also, the Fourier charge density was increased up to $G_{max} = 12(\text{a.u.})^{-1}$. The Monkhorst–Pack scheme in the Brillouin zone is realized with 1500 special k-points of the $Mn_{n+1}SiC_n$, $n = 1, 2, 3$ compounds [38]. The states of Mn: $3p^6 3d^5 4s^2$, Si: $3s^2 3p^2$ and C: $2s^2 2p^2$ were treated as valence

states, respectively. During the self-consistent convergence of the total energy was set at 0.1 mRy.

3. Results and discussion

3.1. Structural properties

3.1.1. Lattice parameters and bulk modulus

The phases $Mn_{n+1}SiC_n$, $n = 1, 2, 3$ like most Max phases crystallize in the space group of P63/ mmc with hexagonal structure. The unit cell contains 8,12, and 16 atoms for Mn_2SiC, Mn_3SiC_2, and Mn_4SiC_3 respectively, and the equivalent atomic positions for n = 1, 2 and 3, are calculated from the data available in references [39] for n = 1, [10] for n = 2, and [12] for n=3. Thus, the higher-order MX layers in the primitive cell increase with increasing n. The structure of the MAX phases is described by three parameters a, c, and the free internal parameter Z_M. The free internal parameter denoted Z_M, defines the distance between the Manganese element, and the plane of the carbon atoms, its formula as follows $Z_M = \frac{Z_M}{C}$ [40]. This parameter influences the octahedral distortion of carbon atoms with respect to cubic symmetry. In this study, atomic positions, (c/a) ratio and lattice parameters were relaxed for each structure. The coordination positions of the different atoms for the three compounds are shown in Table 1. We determined the magnetic stability of the compounds $Mn_{n+1}SiC_n$, $n = 1 - 3$, by the energy difference between the NM configuration, and the FM configuration by applying the following relation $\Delta E = E_{PM} - E_{FM}$ with E_{PM}, and E_{FM} are respectively the energies of the paramagnetic (PM), and FM configurations. The properties of the ground state of the Max phases, $Mn_{n+1}SiC_n$, $n = 1 - 3$ are determined by fitting the Murnaghan equation of state [41], which describes the total energy as a function of volume. First, we minimized the free internal parameters Z_M by taking random parameters to begin our calculations because there is no indication of this subject. We, therefore, performed detailed structural optimizations, minimizing all energies. Our results of the computed lattice constants, a and c, compressibility modulus B, and their derivatives B' of FM, and NM configurations, are summarized in Table 2. In Table 1, we present the optimized values of the free internal parameters in the functional for the three compounds. The minimum energy-optimized, the formation energy, and cohesive energy are presented in Table 2 with FM, and NM configurations. While the results of the structural optimization for $Mn_{n+1}SiC_n$, $n = 1 - 3$, are shown in Fig. 2. We found that the energy difference (ΔE) between PM, and FM was equal to 0.24, 0.87 and 1.04 eV for n = 1, n = 2, and n = 3, respectively. These values are positive, indicating that the FM configuration is more stable than the NM configuration. From the results of Table 2, we can conclude that the ratio (c/a) is in good agreement with other calculations of the same family [13, 42–44]. We also see that the (c/a) ratio is growing from 4.06 to 5.68, to 7.2 for Mn_2SiC, Mn_3SiC_2, and Mn_4SiC_3 with the increase in the compressibility modulus of different Max phases $Mn_{n+1}SiC_n$, $n = 1 - 3$. We see the absence of theoretical results reported in the literature for comparison, our calculated values must be considered as the first prediction.

Table 1 The Wyckoff positions of the Max phases $Mn_{n+1}SiC_n$ for n = 1, 2 and 3

Mn_2SiC	Mn	1/3	2/3	Z_{mn} = 0.0906 (present)
	Si	1/3	2/3	3/4
	C	0	0	0
Mn_3SiC_2	Mn_1	0	0	$Z_{Mn_1} = 0.635$(present)
	Mn_2	1/3	2/3	$Z_{Mn_2} = 0.865$(present)
	Si	0	0	1/4
	C	1/3	2/3	$Z_C = 0.924$(present)
Mn_4SiC_3	Mn_1	1/3	2/3	$Z_{Mn_1} = 0.657$(present)
	Mn_2	0	0	$Z_{Mn_2} = 0.843$(present)
	Si	1/3	2/3	1/4
	C_1	0	0	0
	C_2	2/3	1/3	$Z_{C_2} = 0.885$(present)

3.1.2. Formation and cohesive energy

To check the relative stability of the Max phases $Mn_{n+1}SiC_n$, $n = 1 - 3$,we calculated the formation energy using the following relation [7, 45, 46].

$$E_{Form}^{Mn_{n+1}SiC_n} = \frac{E_{total}^{Mn_{n+1}SiC_n} - \left[xE_{solid}^{Mn} + yE_{solid}^{Si} + zE_{solid}^{C}\right]}{x + y + z} \quad (1)$$

with x, y, and z are the numbers of atoms Mn, Si, and C in the unit cell, respectively. We used (x = 4, y = 2 and z = 2) for n = 1, (x = 6, y = 2 and z = 4) for n = 2 and (x = 8, y = 2 and z = 6) for n = 3, with $E_{total}^{Mn_{n+1}SiC_n}$ is the total energy of the compound, and E_{solid}^{Mn}, E_{solid}^{Si}, E_{solid}^{C} correspond to the energy of each atom when they are crystallized, With, Mn crystallizes in a centered cubic structure (space group $Im\bar{3}m$, prototype W), and Si crystallizes in a face-centered cubic structure (space group $Fm\bar{3}m$, prototype Cu), and C crystallizes in a diamond structure (space group $Fd\bar{3}m$). The formation energy has negative values of – 0.248, – 0.11, and – 0.76 eV/atom for Mn_2SiC, Mn_3SiC_2, and

Table 2 Calculated values for the lattice parameter a, and c, c/a, bulk modulus B(Gpa) and their pressure derivatives (B'), the minimum total energies (E_{eq}), formation energy E_{Form}(eV/atom), cohesive energy E_{coh}(eV/atom) for Max phases $Mn_{n+1}SiC_n$ for n = 1, 2, and 3

	a (Å)	c (Å)	c/a	B	B'	E_{Form}	E_{Coh}	E_{eq} (Ry)
Mn_2SiC								
FM	2.76	11.22	4.06	261.07	4.72	− 0.248	− 54.8	− 10559.91834
NM	2.75	11.6	4.22	287.2	4.27	− 0.219	− 54.34	− 10559.90099
Mn_3SiC_2								
FM	2.78	15.78	5.68	284.6	4.56	− 0.11	− 84.72	− 15337.30075
NM	2.82	15.79	5.6	293.44	4.24	− 0.04	− 83.55	− 15337.23683
Mn_4SiC_3								
FM	2.80	20.2	7.2	280.3	4.36	− 0.76	− 114.56	− 20114.59362
NM	2.81	20.21	7.1	330.04	4.57	− 0.69	− 113.04	− 43146.81804

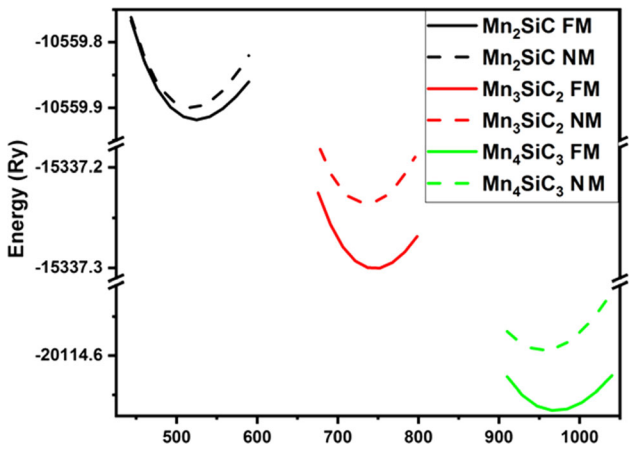

Fig. 2 Total Energy Vs Volume of $Mn_{n+1}SiC_n$, $(n = 1, 2$ and $3)$

Mn_4SiC_3 respectively, which are shown in Table 2, which means that the compounds $Mn_{n+1}SiC_n, n = 1 - 3$, are stable in hexagonal ferromagnetic phases, and the probability of synthesizing it experimentally. To confirm the structural stability of the phases Max $Mn_{n+1}SiC_n$, $n = 1 - 3$, we calculated the cohesive energy. Therefore, the cohesive energy of a solid is the energy that must be provided to separate it into its constitutions in the free state. The cohesive energy of a compound is defined as the total equilibrium energy of the compound minus the total energy of the constituent atoms, using the following equation: [47–49].

$$E_{coh}^{Mn_{n+1}SiC_n} = E_{total}^{Mn_{n+1}SiC_n} - \left[xE_{atom}^{Mn} + yE_{atom}^{Si} + zE_{atom}^{C}\right] \quad (2)$$

with $E_{Coh}^{Mn_{n+1}SiC_n}$ represented the total energy of $Mn_{n+1}SiC_n$, $n = 1, 2, 3$ in the equilibrium configuration, and E_{atom}^{Mn}, E_{atom}^{Si}, and E_{atom}^{C} are the isolated atomic energies of the pure constituent. The isolated atomic energies are calculated using the wien2k code [37]. We determined the energies of the individual atoms by increasing the unit cell of a face-centered cubic structure up to 30 Bohr (about 16 Å) [50]. According to the cohesive energy values, which are listed in Table 2, the FM configuration is the most stable for the three materials due to the lowest cohesive energy (− 54.8, − 84.72, and – 114.56 eV) for the compounds Mn_2SiC, Mn_3SiC_2, and Mn_4SiC_3, respectively. This result confirms the structural stability of the optimization part.

3.1.3. *Magnetic properties*

The Manganese in different modes of symmetry exhibits different magnetic moments due to contact with different atoms in the stacking sequence. The Mn atom has only one equivalent position in the Mn_2SiC compound which has a moment equal to 0.73 μB. Thus for the other compounds, Mn_3SiC_2 and Mn_4SiC_3 have two unequal positions of (Mn): atoms of Mn $_1$, and Mn $_2$. The calculated total and partial magnetic moments per atom unit cell of $Mn_{n+1}SiC_n$, n = 1, 2, 3 are presented in Table 3. It shows that the ferromagnetic state is revealed by the total positive magnetic moment (2.98 μB, 4.71 μB, and 9, 01 μB) for the three compounds Mn_2SiC, Mn_3SiC_2, and Mn_4SiC_3 respectively, come from the main contribution of the total magnetic moment of the Mn atom. Further remarks the values of the total magnetic moment are increased with the increase in the value of n, this confirms the magnetic nature of the phase max $Mn_{n+1}SiC_n$. We also have the existence of weak anti-ferromagnetic coupling between the principal magnetic moment of the atom (Mn), and the negative magnetic moment of the atoms (Si), and the (C) for all three compounds. Moreover, we observed that the magnetic moment of the position Mn $_1$, is greater than the magnetic moment of the position Mn $_2$ in the two compounds Mn_3SiC_2, and Mn_4SiC_3.

Table 3 Calculated Elastic constants C_{ij}, Bulk modulus B , shear modulus G, Young's modulus E (all in GPa), Poisson's ratio ν, the bulk-modulus -to- shear-modulus ratio, elastic anisotropic factors A_1, A_2, and A_3, linear compressibility ratio, total and partial magnetic moments per atom unit cell (in Bohr magneton μ^B), and in the interstitial site for $Mn_{n+1}SiC_n$, n =1, 2 and 3

	Mn_2SiC	Mn_3SiC_2	Mn_4SiC_3
C_{11}	184.53	281.37	498.82
C_{12}	118.28	178.45	239.02
C_{13}	147.23	163.39	438.46
C_{33}	272.54	319.8	100.92
C_{44}	67.43	143.11	124.71
C_{66}	33.125	51.46	249.4
E	131.1	222.5	300.91
B	157.15	210.21	320.39
G	48.16	84.05	111.99
A_1	0.64	0.52	1.1
A_2	1.3	2.78	0.8
A_3	0.83	1.45	0.89
ν	0.36	0.32	0.34
B/G	3.26	2.5	2.86
$f = \frac{K_c}{K_a}$	0.07	0.85	1.35
μ^{Mn_1}	0.734	1.656	1.592
μ^{Mn_2}	–	0.340	0.669
μ^{Si}	− 0.012	− 0.003	− 0.010
μ^{C_1}	− 0.031	− 0.041	− 0.092
μ^{C_2}	–	–	− 0.050
μ^{inter}	0.134	0.209	0.375
μ^{Total}	2.98	4.71	9.013

3.2. Electronic properties

3.2.1. Band structure

We calculated the electronic band structures of the Max phases $Mn_{n+1}SiC_n$, $n = 1, 2, 3$, for the spin up, and down to their equilibrium lattice constants at different points of high symmetry in the Brillouin zone. The energy band structures exhibit strongly anisotropic features with less scattering along the c-axis (see Fig. 3a–f). The Valence and conduction bands overlap considerably, and many bands are crossing the Fermi level, there is no band gap at the Fermi Level. This finding confirms the metallic character of these materials. The lowest energy states of about (− 15 eV) below the Fermi Level, come from the (C–2s) states, these states are separated from the upper part of the valence band, and it is composed mainly of Mn–3d, C–2p, and Si–3s–3p states. The correct states at the Fermi level are Mn–3d giving rise to the magnetic properties of these compounds, this result confirms the metallicity of these three materials. As a result, the electrical conductivity is anisotropic for these materials, along the c axis, i.e., (H-K), the bands are less dispersive. This can be seen from the relatively non-dispersive nature of the bands as well as the M-K directions in the Brillouin zone. Therefore, the electrical conductivity along the c axis is much lower than in the basal plane. Similar results are found with previous reports on Max phases [7, 9, 10, 31].

3.2.2. Electronic densities of states (DOS)

The total and partial densities of states (DOS and PDOS) for the Max phases $Mn_{n+1}SiC_n$, $n = 1 - 3$ are illustrated in Fig. 4(a–d). For Figure 4(a) we see that there is no gap and the existence of a maximum peak density at the Fermi level. From Fig. 4(b–d), we note that Mn–3d orbitals are the main contributor to DOS at the Fermi level, and should be involved in conduction properties although electrons (3d) are generally considered to be low-efficiency drivers. The electrons Si–3s, and C–2s have low participation at the Fermi level due to an excavation effect resulting from the presence of the 3d states of Manganese. The energy states in the range of – 15 to 0 eV are due to the hybridization of the Mn–3d, Si–3p, and C–2p states. The overlap of these states is evidence of the formation of interatomic (covalent) bonds in these examined materials. The bands around the Fermi level are mainly the Mn–3d states which give rise to the magnetic properties with some presence of the Si–3p states, which are responsible for the metallic character of these compounds. For PDOS the hybridization in these compounds is strongly dominated by the contribution of C–2p, Mn–3d states. On the other hand, we notice a weak hybridization of Si–3p–Mn–3d states. This suggests that the Mn–3d, C–2p bond is stronger than the Mn–3d, Si–3p bond. These results are also in good agreement with the first studies of principles on compounds of the same family [7, 51–55]. Finally, the same remark was already made in the analysis of band structures.

3.2.3. The charge density

The charge density distribution provides detailed information on the interaction between the different atoms, and therefore on the nature of the bonds, namely the covalent, ionic, or metallic character. Figure 5(a–c) shows the contour of the charge densities, of the Max phases $Mn_{n+1}SiC_n$, $n = 1, 2, 3$ located in the basal plane $(11\bar{2}0)$, and density contours binary of the compounds MnC (Fig. 5d) crystallized in the NaCl structure with the (space group $Fm\bar{3}m$), and MnSi (Fig. 5e) crystallized in the cubic structure ($F\bar{4}3m$ space group). The covalent bonds in the

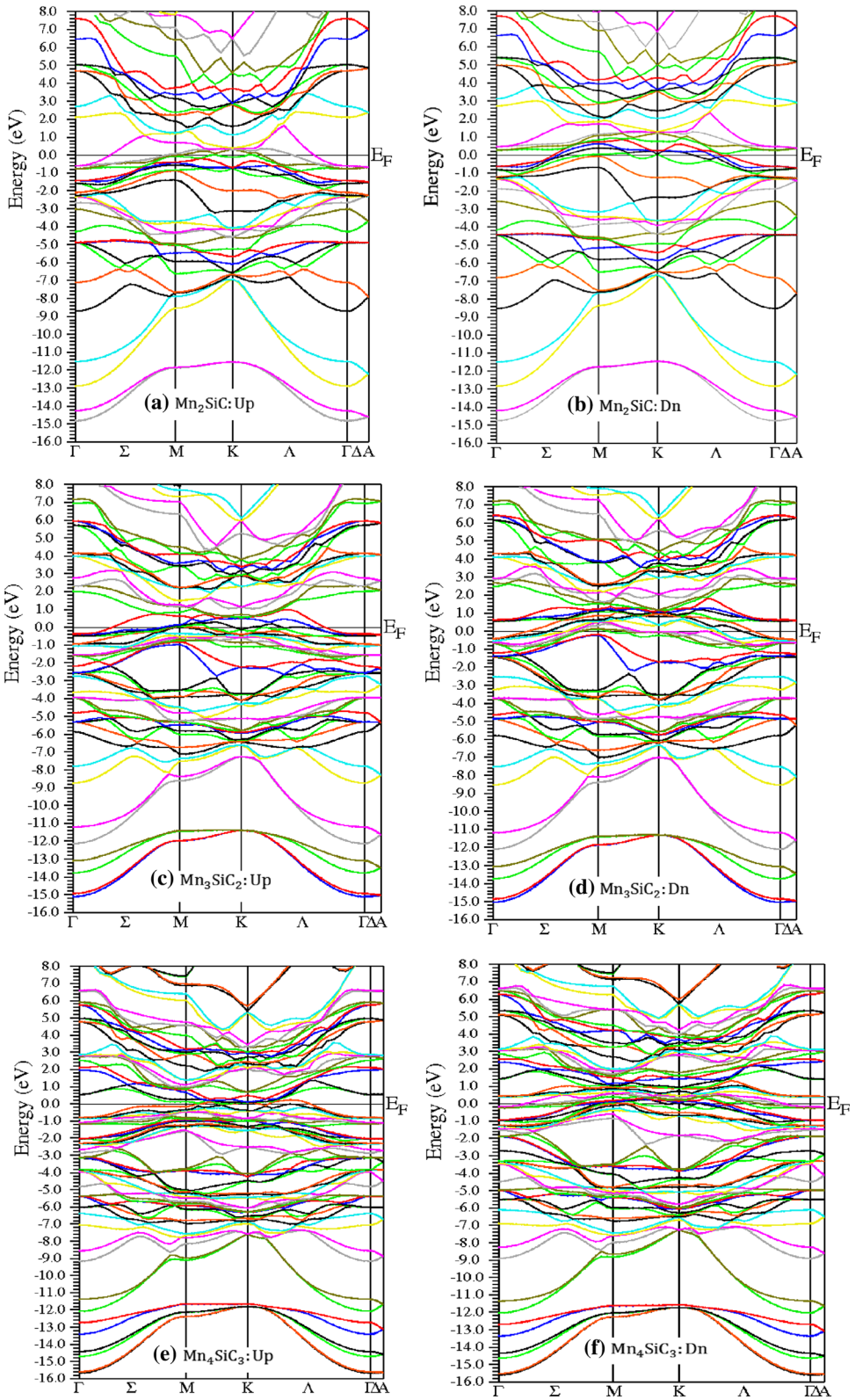

Fig. 3 The calculated band structure of $Mn_{n+1}SiC_n$, (**a**), (**b**) $n = 1$, (**c**), (**d**) $n = 2$ and (**e**), (**f**) $n = 3$

Max phases $Mn_{n+1}SiC_n$, $n = 1, 2, 3$ can be determined from the difference in electronegativity between the elements in play. The p–d interactions of the MnC in $Mn_{n+1}SiC_n$, $n = 1, 2, 3$, Mn (electronegativity of Mn = 1.5) [56], and C (electronegativity of C = 2.55) [56] is covalent in nature and is quite strong (Fig. 5a–c). Therefore, the

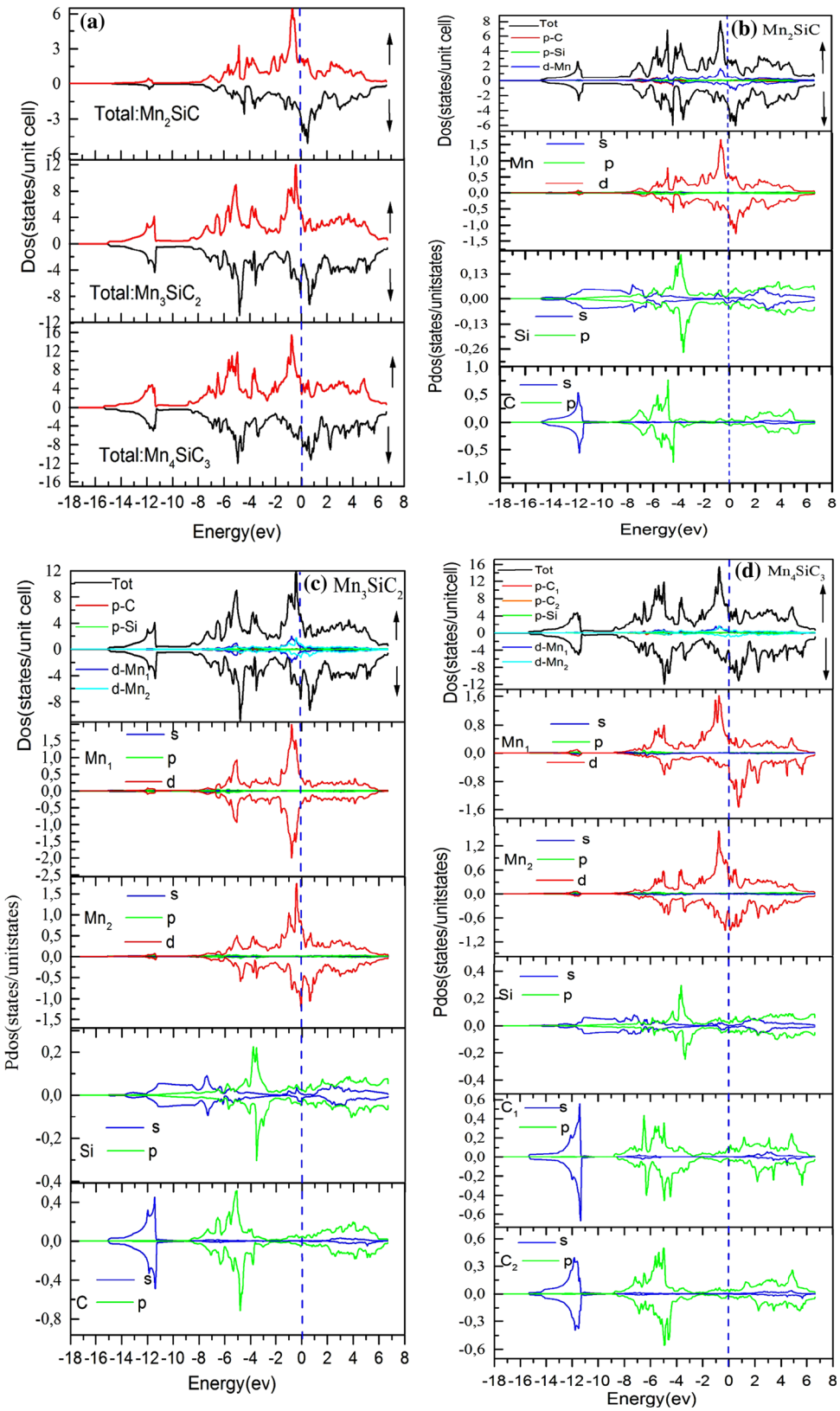

Fig. 4 Total and partial density of states of $Mn_{n+1}SiC_n$, (**a**) Total, (**b**) $n = 1$, (**c**) $n = 2$, and (**d**) $n = 3$.The Fermi level is set to zero energy and marked by a vertical dashed line

strong nature of the covalent bond (Mn–C) in Mn_2SiC, (Mn_2–C–Mn_1–C–Mn_2) in Mn_3SiC_2, and (Mn_2–C_2–Mn_1–C_1–Mn_1) in Mn_4SiC_3 comes from the strong accumulation of charges between them of the Mn, and C atoms. While

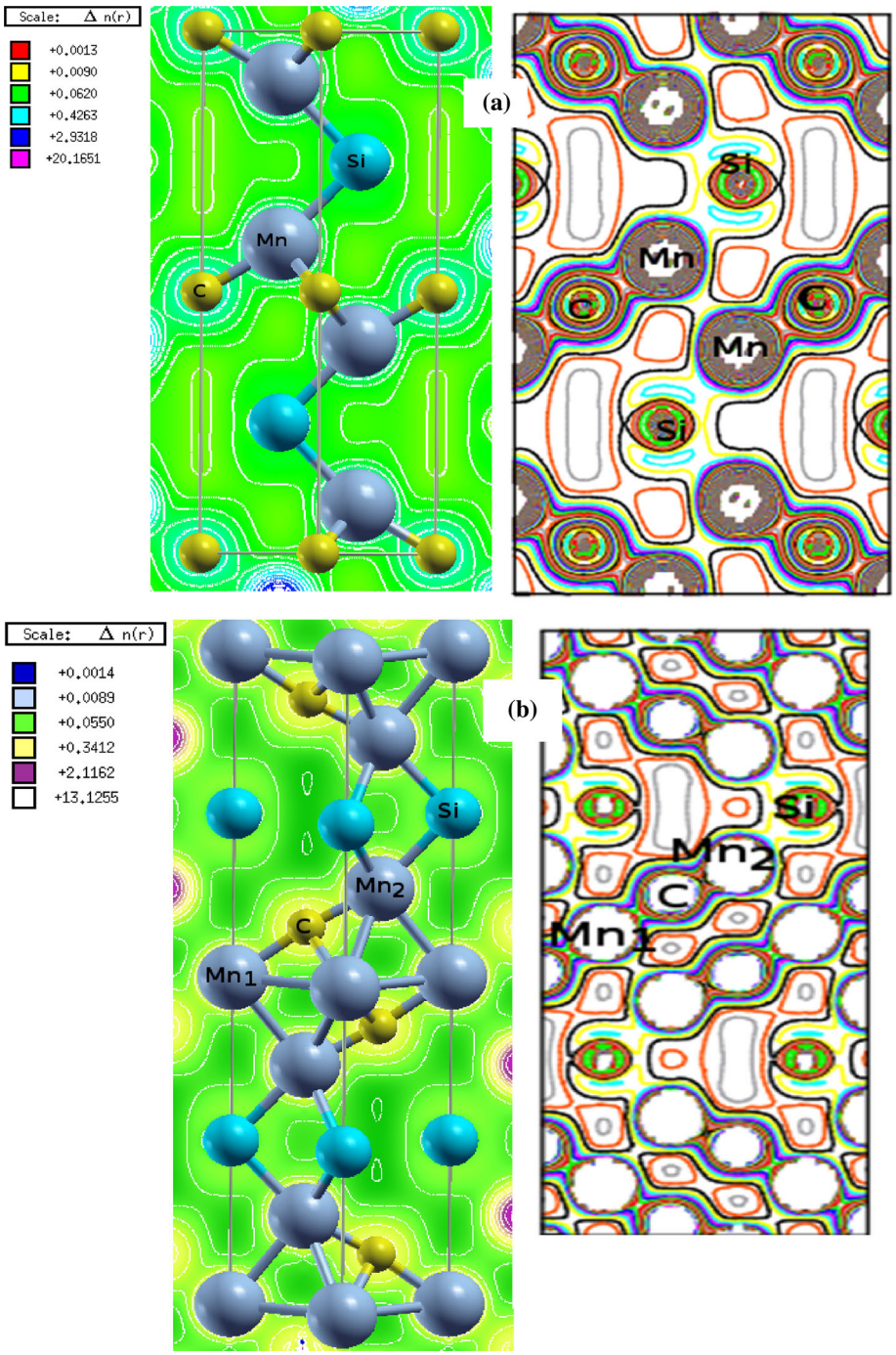

Fig. 5 Charge-density contours for: (**a**) Mn_2SiC, (**b**) Mn_3SiC_2, (**c**) Mn_4SiC_3. Cuts are made in the $(11\bar{2}0)$ plane ,and binary (**d**) MnC, (**e**) MnSi

the carbon atom is more electronegativity than Mn, confirms the presence of an ionic bond between Mn and C Fig. 5(d). The ionic component results from a charge transfer of Manganese to other atoms (Silicon (electronegativity of Si = 1.8) [56], and the more electropositive nature of Silicon confirms the ionic bond between the Manganese, and the Silicon (Fig. 5e). The charge density is taken from the Manganese atoms to the carbon and silicon atoms, this action is due to the difference in electronegativity, the carbon, and silicon atoms. Therefore, the chemical bond in $Mn_{n+1}SiC_n$, $n = 1, 2, 3$ is metallic, covalent ,and ionic in nature. The covalent bond is due to the local interactions of the hybridization Mn–3d and C–2p, and the ionic bond is relative to the local interactions of the hybridization Mn–3d, and Si–3p. In addition, the chemical bond in $Mn_{n+1}SiC_n$, $n = 1, 2, 3$ is anisotropic with the metal band in the Manganese and Silicon layers which are parallel to the basal plane Fig. 5(e), while there are strong directional covalent and ionic bonds between the (Manganese, Carbon) and (Manganese, Silicon). This

Fig. 5 continued

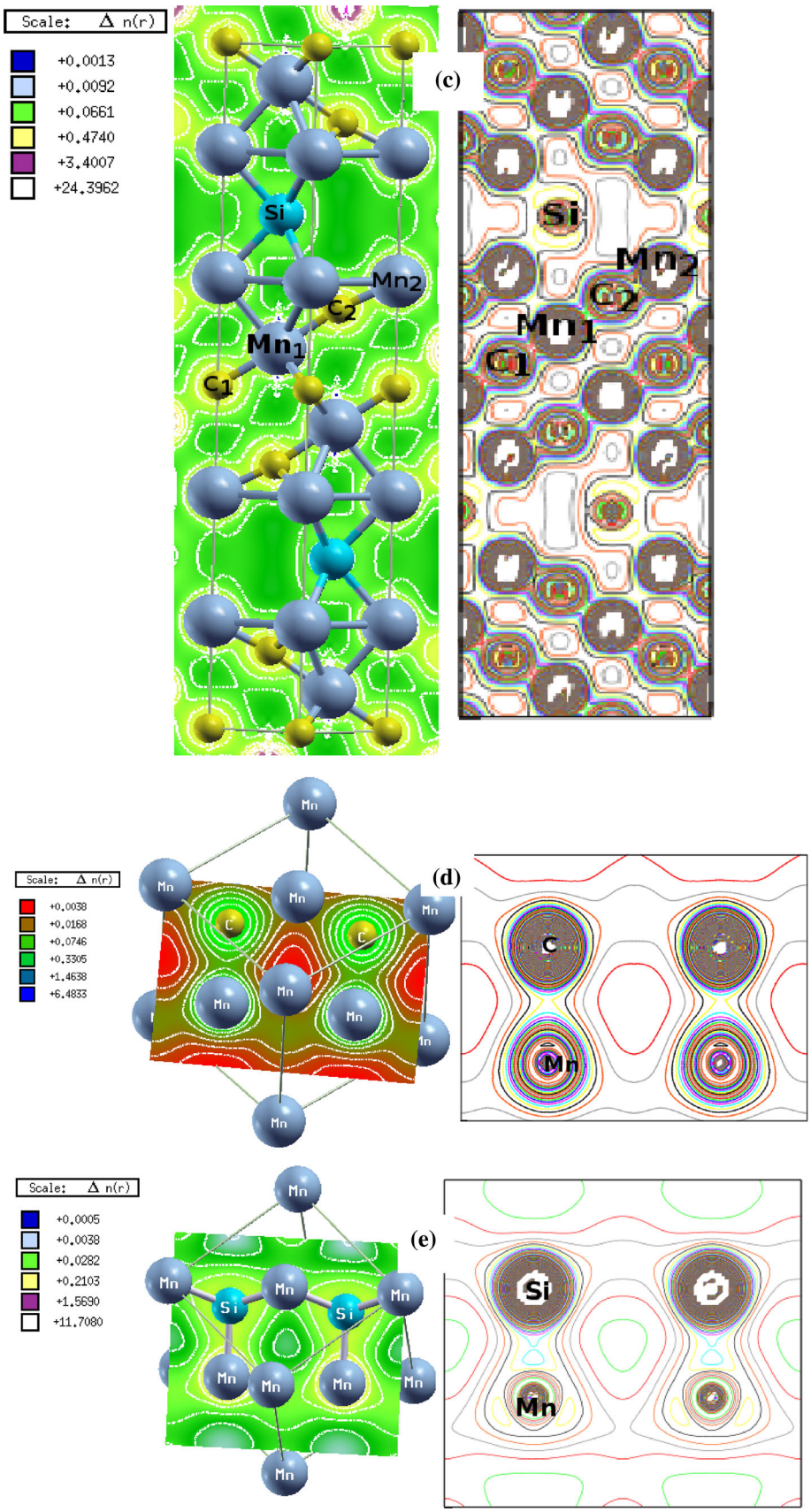

strong anisotropy of the chemical bond is related to the physical and mechanical properties of the placed materials, the high melting points and large compressibility modulus are expected from the strong covalent and ionic bond, while good electrical conductivity and plasticity are expected from the existence of the metallic bond between manganese and silicon in the structure [57]. The same trend was confirmed by the work of Barsoum [3], Sun and Zhou [12], Sun [58], and Zhou [59].

3.3. Elastic properties

To determine the mechanical stability we have calculated the elastic constants under deformation. The elastic constants are macroscopic quantities relating to homogeneous solids. The elastic constants C_{ij} allow access to more important information than that obtained from total energy calculations concerning the ground state of a given system. using the method developed by Reshak, and Morteza [60], integrated with the wien2k code [37] to study the elastic and mechanical properties of the Max phases $Mn_{n+1}SiC_n$, $n = 1 - 3$. The hexagonal crystal structure has five independent elastic constants C_{11}, C_{12}, C_{13}, C_{33}, C_{44}, in addition to the sixth constant C_{66} defined by $C_{66} = (C_{11} - C_{12})/2$. The Criterion of mechanical stability is [61, 62].

$$C_{44} > 0, C_{66} = \frac{1}{2}(C_{11} - C_{12}) > 0 \text{ and } C_{11} + C_{12} - \frac{2C_{13}^2}{C_{33}} > 0 \quad (3)$$

The calculations of the elastic constants of the second order of $Mn_{n+1}SiC_n$, $n = 1, 2, 3$ are presented in Table 3. We observe all the elastic constants are positive and verify the criterion of mechanical stability [62]. Besides, all the values of the elastic constants are increased with the increase in the value of n, the elastic constants C_{11} and C_{33}, are related respectively to the directions a and c, and represent the rigidity compared to the principal strains, while C_{44} is related to the shear stress. We note that C_{44} is lower than C_{11}. In addition C_{33}. $C_{11} + C_{12} > C_{33}$ means that the bonding force and the tensile modulus of elasticity are greater than those along the c-axis in direction (001) . This indicates that the shear strain is easier than linear compression along the crystallographic axes a and c [9]. To understand the mechanical properties, we calculated the moduli (E, B, and G), B/G (Pugh ratio), Poisson's ratio (ν), and the elastic anisotropy index (A_1, A_2, A_3). The values obtained are listed in Table 3. Young's modulus E, and the Poisson ratio are calculated by using the relationships: $E = 9BG/(3B + G)$ et $v = (3B - 2G)/2(3B + G)$ [9, 63], with the compressibility modulus (B), represents a measure of the resistance of a material to the variation in volume by applied pressure, and the shear modulus G defines the measure of a material's resistance to elastic shear deformation, it is lower than the corresponding compressibility modulus B. This can be explained by the lamellar structure of the Max phases, and the young modulus determines the rigidity of a material. We notice that there are no available data to compare with our results of elastic constants, bulk, and shear modulus. From these results, we can say that all the values increase as a function of the growth of the values of n. The Poisson's ratio ϑ for brittle materials has values less than 0.26, while it behaves as values greater than 0.26 for ductile materials [24, 64]. The compounds Mn_2SiC, Mn_3SiC_2, and Mn_4SiC_3 have Poisson ratios $\vartheta = 0.36, 0.32$, and 0.43, respectively greater than the value 0.26, so they are ductile materials. According to Pugh's criteria [65, 66], a material must behave in a ductile, if the B/G ratio is greater than 1.75, if not it must be brittle, for our materials the values are greater than 1.75, therefore our compounds are ductile in nature. The three independent shear anisotropy factors for hexagonal crystals exhibit the degree of anisotropy in bonding between atoms in different planes, which can be defined [57, 67].

$$A_1 = \frac{\frac{1}{6}(c_{11} + c_{12} + 2c_{33} - 4c_{13})}{c_{44}},\ A_2 = \frac{2c_{44}}{c_{11} - c_{12}},\ A_3 = A_1 \cdot A_2 = \frac{1/3(\ c_{11} + c_{12} + 2c_{33} - 4c_{13})}{c_{11} - c_{12}} \quad (4)$$

and any deviation greater or less than 1 corresponds to an elastic anisotropy while any equal to one corresponds to an isotropic crystal. Moreover, the compressibility anisotropic factor (k_c/k_a) for the hexagonal crystal is defined by the ratio between the linear compressibility coefficients along with the c- and a-axis, it is definite by the following relation [50, 55].

$$\frac{K_c}{K_a} = \frac{C_{11} + C_{12} - 2C_{13}}{C_{33} - C_{13}} \quad (5)$$

The results obtained for k_c/k_a are 0.07, 0.85, and 1.35 for Mn_2SiC, Mn_3SiC_2, and Mn_4SiC_3, respectively. These results demonstrate that the compressibility for Mn_4SiC_3 with the (c) axis is greater than along the (a), but $k_c/k_a =$ 0.07 for Mn_2SiC, indicates that the compressibility along the axis (c) is smaller than along axis a for Mn4sic3 and Mn_3SiC_2.

3.4. Thermodynamic Properties

In this study, the thermal properties of $Mn_{n+1}SiC_n$, $n = 1 - 3$, are calculated from the quasi-harmonic approximation (QH) was analyzed using Gibbs2 [68–70] in the temperature range from 0 to 1200 K because this model

demonstrates its perfect suitability in this range. This model is successfully applied to the study of different materials [7]. To calculate these properties we used the results of the energy part versus volume of the optimization as input, using the FP-LAPW method in the LDA approximation, which involves the model-based analysis QH Debye [68, 70, 71]. The mass modulus (B), the change in volume (V), the heat capacity (C_V), and the Debye temperature (θ_D) for $Mn_{n+1}SiC_n$, $n = 1 - 3$, are designated according to temperature, which are shown in Figures 6, 7, 8, 9. From Fig. 6, it can be seen that there is a negligible variation in volume with a temperature up to about 200 K, at -above this temperature, the volume increases monotonically up to high temperatures. The relationship between mass modulus B and temperature is shown in Fig. 7. We see that the mass modulus B has a constant value which is approximately (518.2, 566.4, and 597.4 Gpa) for n = 1-3, respectively in the range 0–150 K. When the temperature increases, the mass modulus B also decreases monotonically. For Fig. 8, the Debye temperature is practically constant at $T < 200$ K, it has a value of approximately 1097.9, 1013.4, and 950.7 K for n = 1, n = 2, and n = 3 respectively, and the decrease, directly when the temperature goes from 200 to 1200 K. The study of the thermal capacities of C_V as a function of the temperature at constant pressures is represented in Fig. 9. At very low temperatures (0 k), C_V increases rapidly, and we note that when $T < 1150$ K (C_V is proportional to T^3) for the three materials, the specific heat capacity is (70.2 J mol^{-1} K^{-1}) in these three compounds.

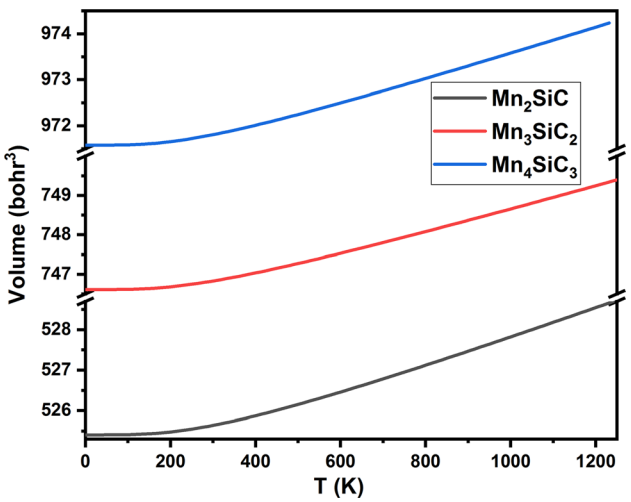

Fig. 6 Volume verses temperature plots with LDA approximation for $Mn_{n+1}SiC_n$

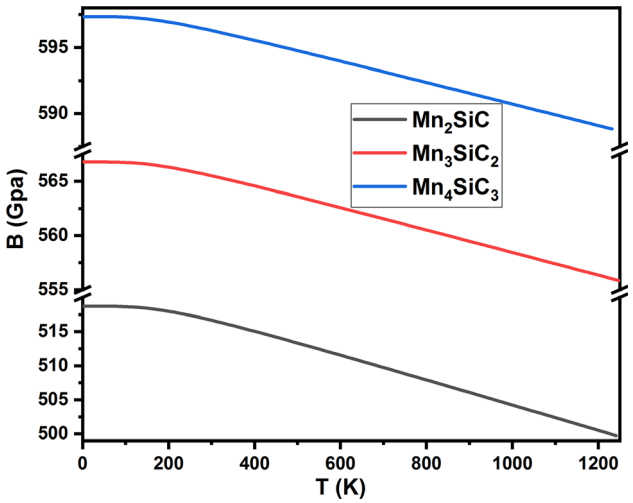

Fig. 7 Bulk modulus verses temperature plots with LDA approximation for $Mn_{n+1}SiC_n$

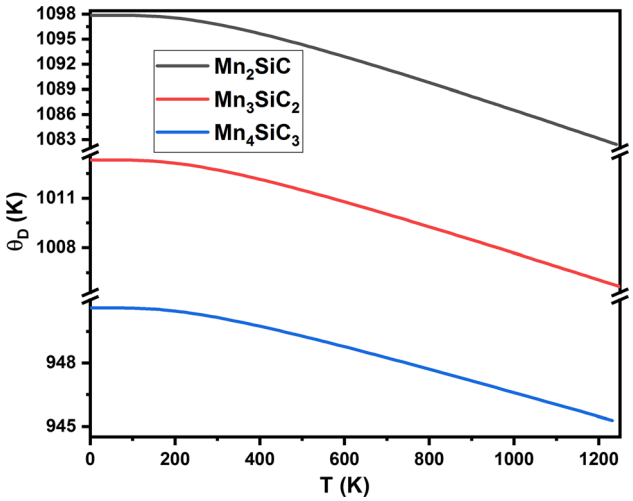

Fig. 8 Debye temperature verses temperature plots with LDA approximation for $Mn_{n+1}SiC_n$

4. Conclusions

In summary, we have used the calculations of the first principle of DFT based on the FP-LAPW method by applying the local density approximation LSDA to calculate the structural, electronic, elastic, magnetic, and thermodynamic characteristics for the Max phases. $Mn_{n+1}SiC_n$, $(n = 1, 2$ and $3)$. Our calculated results showed that $Mn_{n+1}SiC_n$, $(n = 1, 2$ and $3)$ are more stable because their formation energy values are negative, which allows us to say that the synthesis of these compounds can be carried out. We have also found that the ferromagnetic arrangement of the Max phase $Mn_{n+1}SiC_n$, $(n = 1, 2$ and $3)$ is more favorable than the Nonmagnetic configuration. Stability in the ferromagnetic configuration is confirmed by the calculation of the

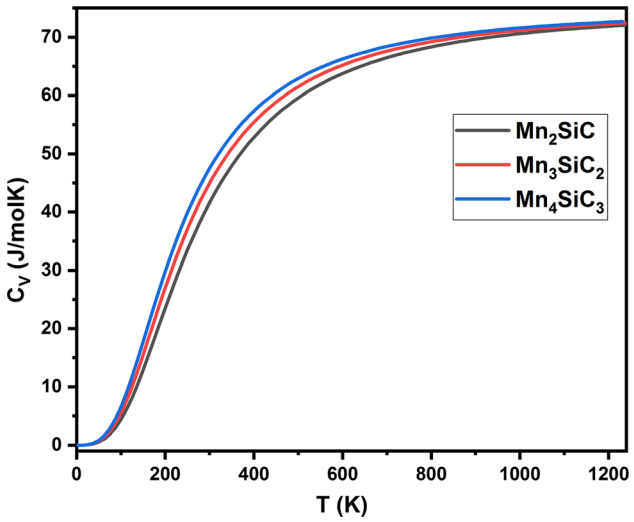

Fig. 9 Constant volume heat capacity verse temperature with LDA approximation for $Mn_{n+1}SiC_n$

cohesive energy. All investigated Max phases satisfied the Born criteria for mechanical stability. The origin of ferromagnetism in Max phases $Mn_{n+1}SiC_n$ is mainly due to the participation of the 3d states of manganese. The density of the states, also showed that these studied MAX phases are conductors, with a major contribution coming from the electronic states Mn-3d. PDOS shows another interesting feature, the hybridization peak of Mn–3d and C–2p states is stronger than that between Mn–3d and Si–3p states in the low energy range. Furthermore, the Mn–3d, C–2p bonds are more rigid than the Mn–3d, Si–3p bonds. Regarding the thermodynamic properties of the Max phases $Mn_{n+1}SiC_n, (n = 1 - 3)$, the volume increases linearly with an increase in temperature, while the mass modulus decreases with an increase in temperature. The heat capacity C_V increases rapidly up to a temperature of 1150 K, then remains constant for all three compounds. Mn_2SiC, Mn_3SiC_2, and Mn_4SiC_3 can be used for many technological applications as materials of structure at high temperatures. Since this is the first study done on these three compounds, we generally believe that our results provide predictions for experimenters to explore this new class in their experimental studies in future.

References

[1] Z Sun, R Ahuja, and J M Schneider *Phys. Rev. B* **68** 224112 (2003)
[2] P Eklund, M Beckers, U Jansson, H Högberg, and L Hultman *Thin Solid Films* **518** 1851 (2010)
[3] M W Barsoum *Prog. Solid State Chem.* **28** 201 (2000)
[4] M W Barsoum and T El-Raghy *J. Am. Ceram. Soc.* **79** 1953 (1996)
[5] Y Medkour, A Roumili and D Maouche *Eur. Phys. J. Appl. Phys.* **44** 125 (2008)
[6] W Jeitschko, H T Nowotny and F Benesovsky *J. Less Common Met.* **7** 133 (1964)
[7] H Mebtouche et al *Mater. Today Commun.* **25** 101420 (2020)
[8] F Sultana, M M Uddin, M A Ali, M M Hossain, S H Naqib, and A Islam *Results Phys.* **11** 869 (2018)
[9] M Roknuzzaman, M A Hadi, M A Ali, M M Hossain, N Jahan, M M Uddin, J A Alarco and K Ostrikov *J. Alloys Compd.* **727** 616 (2017)
[10] Y C Zhou, X H Wang, Z M Sun and S Q Chen *J. Mater. Chem.* **11** 2335 (2001)
[11] J Wang, J Wang, Y Zhou, Z Lin and C Hu *Scr. Mater.* **58** 1043 (2008)
[12] Z Sun and Y Zhou *J. Phys. Soc. Japan* **71** 1313 (2002)
[13] Y Bai, X He, Y Li, C Zhu, and M Li *Solid State Commun.* **149** 2156 (2009)
[14] M Magnuson, M Mattesini, S Li, C Höglund, M Beckers, L Hultman, and O Eriksson *Phys. Rev. B* **76** 195127 (2007)
[15] P Finkel *J. Appl. Phys.* **87** 1701 (2000)
[16] J M Schneider, R Mertens and D Music *J. Appl. Phys.* **99** 13501 (2006)
[17] M Naguib et al *Mater. Res. Lett.* **2** 233 (2014)
[18] D Horlait, S Grasso, A Chroneos and W E Lee *Mater. Res. Lett.* **4** 137 (2016)
[19] H-I Yoo, M W Barsoum, and T El-Raghy *Nature* **407** 581 (2000)
[20] I Kero, R Tegman, and M-L Antti *Ceram. Int.* **37** 2615 (2011)
[21] M M Uddin, M A Ali and M S Ali *Indian J. Pure Appl. Phys.* **54** 386 (2016)
[22] M A Ali, M T Nasir, M R Khatun, A Islam, and S H Naqib *Chinese Phys. B* **25** 103102 (2016)
[23] M A Ali, M R Khatun, N Jahan, and M M Hossain *Chinese Phys. B* **26** 33102 (2017)
[24] M A Ali, M M Hossain, N Jahan, A Islam and S H Naqib *Comput. Mater. Sci.* **131** 139 (2017)
[25] M A Ali et al *J. Alloys Compd.* **743** 146 (2018)
[26] Y Bai, X He, R Wang, S Wang and F Kong *Comput. Mater. Sci.* **91** 28 (2014)
[27] C Zouaneb et al *J. Supercond. Nov. Magn.* 1 (2021)
[28] V Srivastava, N Kaur, R Khenata, and S A Dar *J. Magn. Magn. Mater.* **513** 167107 (2020)
[29] V Srivastava, N Kaur, X Wang, M Mushtaq and S A Dar *Int. J. Energy Res.* **45** 11305 (2021)
[30] M M Uddin, M A Ali, M M Hossain, S H Naqib, and A K M A Islam *Indian J. Phys.* (2021). https://doi.org/10.1007/s12648-021-02050-z
[31] M Mebrek, A Mokaddem, B Doumi, A Yakoubi and A Mir *J. Supercond. Nov. Magn.* **31** 2485 (2018)
[32] Z M Sun *Int. Mater. Rev.* **56** 143 (2011)
[33] A Yakoubi, H Mebtouche, M Ameri and B Bouhafs *Mater. Sci. Appl.* **2** 1383 (2011)
[34] P Hohenberg and W Kohn *Phys. Rev* **136** B864 (1964)
[35] W Kohn and L J Sham *Phys. Rev.* **140** A1133 (1965)
[36] J P Perdew and Y Wang *Phys. Rev. B* **45** 13244 (1992)
[37] P Blaha, K Schwarz, G K H Madsen, D Kvasnicka, and J Luitz *An Augment. Pl. Wave+ Local Orbitals Progr. Calc. Cryst. Prop.* (2001)
[38] H J Monkhorst and J D Pack *Phys. Rev. B* **13** 5188 (1976)
[39] I R Shein and A L Ivanovskii *Phys. B Condens. Matter* **410** 42 (2013)
[40] G Hug, M Jaouen and M W Barsoum *Phys. Rev. B* **71** 24105 (2005)
[41] F D Murnaghan *Proc. Natl. Acad. Sci. U. S. A.* **30** 244 (1944)
[42] W Luo and R Ahuja *J. Phys. Condens. Matter* **20** 64217 (2008)
[43] D Music, R Ahuja and J M Schneider *Appl. Phys. Lett.* **86** 31911 (2005)

[44] M W Barsoum and M Radovic *Annu. Rev. Mater. Res.* **41** 195 (2011)
[45] Z W Huang, Y H Zhao, H Hou and P D Han *Phys. B Condens. Matter* **407** 1075 (2012)
[46] A Yakoubi, O Baraka, and B Bouhafs *Results Phys.* **2** 58 (2012)
[47] O Canko, F Taşkın, M Atiş, N Kervan and S Kervan *J. Supercond. Nov. Magn.* **29** 2573 (2016)
[48] A A M Abadi, G Forozani, S M Baizaee and A Gharaati *J. Supercond. Nov. Magn.* **32** 2479 (2019)
[49] F Ahmadian and R Alinajimi *Comput. Mater. Sci.* **79** 345 (2013)
[50] M Mebrek, A Mokaddem, B Doumi, A Yakoubi, and A Mir *Acta Phys. Pol. A.* **133** (2018)
[51] G Surucu, K Colakoglu, E Deligoz and N Korozlu *J. Electron. Mater.* **45** 4256 (2016)
[52] A Gencer and G Surucu *Mater. Res. Express* **5** 76303 (2018)
[53] M Magnuson et al *Phys. Rev. B* **74** 205102 (2006)
[54] G Surucu, H H Gullu, A Candan, B Yildiz and A Erkisi *Philos. Mag.* **100** 2183 (2020)
[55] J Wang, Y Zhou, T Liao and Z Lin *Appl. Phys. Lett.* **89** 21917 (2006)
[56] L Pauling *J. Am. Chem. Soc.* **54** 988 (1932)
[57] M Mebrek, M Berber, B Doumi and A Mokaddem *Rev. Mex. Física* **67** 500 (2021)
[58] Z Sun, D Music, R Ahuja, S Li and J M Schneider *Phys. Rev. B* **70** 92102 (2004)
[59] Z Sun, Y Zhou and M Li *Corros. Sci.* **43** 1095 (2001)
[60] A H Reshak and M Jamal *Int. J. Electrochem. Sci* **8** 12252 (2013)
[61] J F Nye *Physical properties of crystals: their representation by tensors and matrices* (Oxford university press) (1985)
[62] J Wang, J Wang, Y Zhou, and C Hu *Acta Mater.* **56** 1511 (2008)
[63] M S Islam and A Islam *Phys. B Condens. Matter* **406** 275 (2011)
[64] I N Frantsevich, F F Voronov and S A Bakuta *Kiev Izd. Nauk. Dumka* **1982** 288 (1982)
[65] S F Pugh *London, Edinburgh, Dublin Philos. Mag. J. Sci.* **45** 823 (1954)
[66] S Boucetta *J. Magnes. Alloy.* **2** 59 (2014)
[67] H M Ledbetter *J. Phys. Chem. Ref. Data* **6** 1181 (1977)
[68] S Ghosh and D C Gupta *J. Magn. Magn. Mater.* **411** 120 (2016)
[69] A O de la Roza and V Luaña *Comput. Phys. Commun.* **180** 800 (2009)
[70] M A Blanco, E Francisco and V Luana *Comput. Phys. Commun.* **158** 57 (2004)
[71] A Otero-de-la-Roza, D Abbasi-Pérez and V Luaña *Comput. Phys. Commun.* **182** 2232 (2011)

Publisher's Note Springer Nature remains neutral with regard to jurisdictional claims in published maps and institutional affiliations.